Chemical imaging of sphingolipids and phospholipids at the single amyloid-β plaque level in postmortem human Alzheimer's disease brain

Wojciech Michno[1,2,3], Andrew Bowman[4], Durga Jha[1], Karolina Minta[1], Junyue Ge[1], Srinivas Koutarapu[1], Henrik Zetterberg[1,5,7,8,9], Kaj Blennow[1,7], Tammaryn Lashley[5,6], Ron M.A. Heeren[4], Jörg Hanrieder[1,5,*]

1) Department of Psychiatry and Neurochemistry, Sahlgrenska Academy, University of Gothenburg, Mölndal, Sweden
2) Department of Neuroscience, Physiology and Pharmacology; University College London, London, United Kingdom
3) Department of Pediatrics, Stanford University School of Medicine, Stanford University
4) Maastricht MultiModal Molecular Imaging Institute (M4I), Maastricht University, Maastricht, The Netherlands
5) Department of Neurodegenerative Disease, Institute of Neurology, University College London, London, United Kingdom
6) Queen Square Brain Bank for Neurological Disorders, Department of Clinical and Movement Neurosciences, Institute of Neurology, University College London, London, United Kingdom
7) Clinical Neurochemistry Laboratory, Sahlgrenska University Hospital, Mölndal, Sweden
8) UK Dementia Research Institute, UCL, London, UK
9) Hong Kong Center for Neurodegenerative Diseases, Hong Kong, China

* Correspondence: Dr Jörg Hanrieder,

E-mail: jh@gu.se

ORCID
Jörg Hanrieder, 0000-0001-6059-198X
Wojciech Michno: 0000-0002-3096-3604
Henrik Zetterberg: 0000-0003-3930-4354

SUMMARY

Lipids dysregulations have been critically implicated in Alzheimer's disease (AD) pathology. Chemical analysis of amyloid-β (Aβ) plaque pathology in transgenic AD mouse models has demonstrated alterations in the microenvironment in direct proximity to Aβ plaque pathology. In mouse studies, differences in lipid patterns linked to structural polymorphism among Aβ pathology, such as diffuse, immature, and mature fibrillary aggregate have also been reported. To date, no comprehensive analysis of neuronal lipids microenvironment changes in human AD tissue has been performed.

Here, for the first time we leverage matrix-assisted laser desorption/ionization mass spectrometry imaging (MALDI MSI) though high speed and spatial resolution commercial time-of-light instrument, as well as high mass resolution in-house developed orbitrap system to characterize the lipid microenvironment in postmortem human brain tissue from AD patients carrying Presenilin 1 mutations (PSEN 1) that lead to familial forms of AD (fAD). Interrogation of the spatially resolved MSI data on a single Aβ plaque allowed us to verify nearly 40 sphingolipid and phospholipid species from diverse subclasses being enriched and depleted in relation to the Aβ deposits. This included monosialo-gangliosides (GM), ceramide monohexosides (HexCer), ceramide-1-phosphates (CerP), ceramide phosphoethanolamine conjugates (PE-Cer), sulfatides (ST), as well as phosphatidylinositols (PI), phosphatidylethanolamines (PE), and phosphatidic acid (PA) species (including Lyso-forms). Indeed, many of the sphingolipids species overlap with the species previously seen in transgenic AD mouse models. Interestingly, in comparison to the animal studies, we observed an increased localization of PE and PI species containing arachidonic acid (AA). These finding are highly relevant, demonstrating for the first time Aβ plaque pathology-related alteration in the lipid microenvironment in humans. They provide a basis for development of potential lipid biomarkers for AD characterization and insight into human-specific molecular pathway alterations.

INTRODUCTION

Alzheimer's disease (AD) is responsible for ~70% of dementia cases. As the disease is believed to start more than 20 years before any clinical symptoms appear, there is a need for detailed phenomic characterization[1,2]. The classical hallmarks of AD, amyloid-beta (Aβ) plaque deposition and neurofibrillary tangles made up of phosphorylated tau proteins. Consequently, disease-modulating strategies have historically focused on targeting the peptides involved in these pathologies, the Aβ and tau peptides. Lipids, however, have also been implicated in AD and more specifically in Aβ plaque formation[3]. The ε4 allele of the apolipoprotein E encoding gene (APOE), a lipid transporter, is the most prominent genetic risk factor for developing sporadic AD[4]. Additionally, recent Genome-Wide Association Studies (GWAS) have identified multiple lipid-associated genes as AD risk factors (e.g. TREM2, CLU, ABCA7)[5].

The relevance of lipid microenvironment alteration in the context of single Aβ plaques has also been demonstrated in transgenic AD mouse models. Here, Aβ plaque-specific changes in both sphingolipids and phospholipids have been reported using matrix-assisted laser desorption/ionization (MALDI)-based mass spectrometry imaging (MSI)[6–8]. Moreover, such changes were found to be tied to the structural polymorphism of individual Aβ plaques [6,7]. Still, although unlikely, such lipid alterations could be caused by the aberrant APP/Aβ peptide expression in the majority of the transgenic AD rodent models. Therefore, it is of essential interest to identify human-specific alterations in lipid metabolism that are associated with the Aβ plaque pathology.

To advance our molecular understanding of lipid metabolic alterations in the context of Aβ pathology in human AD, we developed an analytical approach to study the chemical lipid composition of individual Aβ plaques in human AD. We specifically focused our analysis on genetic form of AD, specifically subjects carrying *Presenilin 1* mutations (*PSEN 1*) leading to familial AD (fAD). Herein, we established an MSI protocol capable of sensitive lipid imaging at 10µm across large regions of human brain tissue. Through these combined MSI approaches we demonstrate localization/depletion of nearly 40 sphingolipid and phospholipid species on the level of single Aβ plaques. These findings are highly relevant, demonstrating for the first time Aβ plaque pathology related alteration in lipid microenvironment specifically in human subjects.

METHODS

Patient Characteristics

Human postmortem brain tissue was obtained through the brain donation program at Queen Square Brain Bank for Neurological Disorders (QSBB), Department of Clinical and Movement Neurosciences, Institute of Neurology, University College London (UCL).

The standard diagnostic criteria were used for the neuropathological diagnosis of AD.[9] The demographic and neuropathological classifications are shown in Table 1. The study was conducted in accordance with the provisions of the Declaration of Helsinki and approved by the National Hospital for Neurology and Neurosurgery Local Research Ethics Committee, UCL, UK. Ethical approval from a Swedish panel has been received for the same experiments: DNr 012-t5; 150 416 (Göteborg). For this study no randomization, blinding, preregistration, or sample size calculations were performed. No inclusion or exclusion criteria were applied.

Chemicals and reagents

All chemicals for matrix and solvent preparation were pro-analysis grade and obtained from Sigma-Aldrich (St. Louis, MO, USA). TissueTek optimal cutting temperature compound was purchased from Sakura Finetek (AJ Alphen aan den Rijn, The Netherlands). The ddH_2O was obtained from a milliQ purification system (Millipore Corporation, Merck Millipore, Billerica, MA, USA).

Amyloid Staining

Prior to MALDI analysis fluorescent plaque imaging was performed using luminescent conjugated oligothiophene amyloid probes[10]. In brief, sections were fixed in absolute EtOH for 8 min, partially rehydrated in 70%EtOH for 30 s, and rinsed twice in Phosphate Buffer Solution (PBS) for 30 s. For amyloid staining, 30 min incubation with heptamer-formyl thiophene acetic acid (h-FTAA) (1.5 µM) was used[10,11]. Following staining, tissue was washed three times for 1 min in PBS, and dried at 25°C. Overview imaging was performed using a wide-field microscope (Axio Observer Z1; Zeiss) with a Plan-Apochromat 10×/0.3 DIC objective and a 38 HE-AF488 filter (Ex: BP 479/40; Em: BP 525/50). Prior to MALDI MSI analysis, fluorescent images were imported into FlexImaging (v 5.0; Bruker Daltonics, Bremen, Germany) software at 25% size compression in order to guide MALDI-MSI analysis and (post-MALDI-MSI analysis) into SCiLS Lab (v2019; Bruker Daltonics, Bremen, Germany).

MALDI sample preparation and matrix application

For MALDI imaging of lipids, tissues were washed in 10mM Ammonium formate (AmF) followed by application of 1,5 di-amino-naphthalene (1,5-DAN) matrix using a TM-sprayer (HTX

Technologies, Carrboro, NC, USA). Before spraying, the solvent pump (Dionex P-580, Sunnyvale, CA, USA) was purged with 70% ACN at 500 µL/min for 10 min followed by a manual rinse of the matrix loading loop using a syringe. A matrix solution of 20 mg/mL 1,5-DAN in 70% ACN was sprayed onto the tissue sections with the following instrumental parameters: nitrogen flow (12 psi), spray temperature (80 °C), nozzle height (40 mm), five passes with offsets and rotations, and spray velocity (1250 mm/min), and isocratic flow of 50 µL/min using 70% ACN as pushing solvent.

Mass spectrometry imaging analysis

High speed MALDI-MSI acquisition was performed at 10 µm spatial resolution using a MALDI-TOF instrument (rapifleX, Bruker Daltonics). The MALDI source is equipped with a scanning Smartbeam 3D laser featuring a laser beam diameter of 5 µm. Spectra were acquired using custom laser settings with a resulting field size of 10 µm. The measurements were performed with the laser operating at a frequency of 10 kHz with 20 laser pulses per pixel. Acquisition and subsequent processing were performed using the instrument software FlexImaging 5.0 (Bruker Daltonics). Acquisition of high mass resolution MSI data was performed using an Orbitrap Elite mass spectrometer (Thermo Fisher Scientific GmbH, Bremen, Germany) coupled to a reduced pressure ESI/MALDI ion source (Spectroglyph LLC, Kennewick, WA, USA). Further details on the ion source can be found in previous literature[12]. The 349-nm MALDI laser (Spectra Physics, Mountain View, CA, USA) was operated at a repetition rate of 1000 Hz and pulse energy of ~1.5 µJ. The laser was focused to a spot size/step size of ~20 × 20 µm, mass resolution was chosen to be 120,000 (at *m/z* 400), and a total scan time of 1.05 s/scan and pixel.

Data processing and statistical analysis

The MALDI-TOF MSI data analysis was performed in SCiLS Lab (v. 2019, Bruker Daltonic). The MALDI imaging data were total ion current (TIC) normalized. Cluster analysis-based spatial segmentation (bisecting k-means) was used to identify characteristic lipid distributions and for region of interest (ROI) annotation. Nearly 100 Aβ plaques were annotated as ROIs for each of the patients. The Aβ plaque ROIs were exported as *.csv. This was followed by binning analysis for data reduction. Here, all ROI data were imported into Origin (v. 8.1 OriginLab) and peaks and peak widths were detected on the average spectra of each ROI using the implemented peak analyzer function. Bin borders for peak integration were exported as tab-delimited text files and were used for area under curve peak integration within each bin (peak-bin) of all individual ROI average spectra using an in-house developed R script. Single pixel signal correlation (SPSC) of

individual lipid signals for each of the identified species was performed directly in SCiLS Lab (v. 2019, Bruker Daltonic).

The orbitrap data visualization and data analysis was performed using LipostarMSI (Molecular Horizon Srl, Bettona, Italy). MSI *.raw data (Thermo Fisher Scientific GmbH, Bremen, Germany) were converted into imzML[13] by first converting *.raw data into mzML using msconvert (ProteoWizard)[14]. Using the in-built converter of LipostarMSI, the mzmL file was then combined with the positioning file created by the MALDI/ESI injector to generate a profile-mode imzML file. Lipid identification within LipostarMSI was performed with reference to the LIPIDMAPS database[15] and was based on accurate m/z matching using a tolerance of ± 2 ppm and reference to previous literature[16]. Phospholipids, sphingolipids, and sterols were considered for identification.

RESULTS

Mass spectrometry imaging delineated lipid microenvironment of individual Aβ plaques in human AD brain tissue.

To study the lipid microenviroment of Aβ plaque pathology we established a mass spectrometry imaging approach allowing for 10µm analysis of fresh frozen postmortem human brain tissue. Following sequential cryo-sectioning of PSEN subjects, we stained one of the adjacent sections using Aβ amyloid specific stain (Figure 1A (top)). This staining was used as guidance for identification of Aβ plaque-rich regions for subsequent MSI experiments. Further, this allowed us to later verify that the observed MALDI-MSI signal could indeed be attributed to microenvironment changes that are local to the Aβ plaque pathology. Then, the adjacent glass slide was coated with 1,5-DAN matrix followed by lipid imaging using MALDI TOF MSI (Rapiflex, Figure 1A (middle)).

To verify the putatively assigned lipid species, high mass-resolution analysis was performed on an Orbitrap Elite mass spectrometer coupled to a reduced pressure ESI/MALDI ion source (Figure 1A (bottom)). Slides adjacent to the ones analyzed in the MSI experiments were stained using Aβ amyloid-specific stain to verify that the signal observed in MALDI-MSI could be attributed to microenvironment changes that are local to the Aβ plaque pathology.

Initial inspection of the mass spectra acquired from the AD patient's postmortem brain tissue revealed a rich diversity of lipid species (Figure 1B). We performed spatial segmentation using cluster analysis (bisecting k-means) to delineate lipid signature of individual Aβ plaques that distinguish these pathological features from the local tissue lipid environment. Indeed, the clustering analysis identified unique Aβ plaque resembling features (Figure 1D). To verify the

nature of these putative amyloid plaque features, we aligned the MALDI-MSI pseudocluster images of individual patients with the corresponding microscopy images from adjacent tissues that were stained with amyloid specific fluorescent probes (Figure 1E). Here, a high correlation between both MALDI-MSI and amyloid specific fluorescent staining data was observed. We therefore proceeded with defining the identified pseudoclusters as region of interests (ROIs) corresponding to Aβ plaques. These ROI contained species that were both enriched (e.g. GM1(d18:1/18:0)) (Figure 1F) or depleted (ST(d18:1/24:0)) (Figure 1G). Interrogation of the m/z values underlying the pseudoclusters obtained from k-means clustering demonstrated localization of nearly 100 species that were either enriched or depleted in the Aβ plaque ROIs. We were able to verify the identity of nearly 40 of these species using high-mass resolution MALDI orbitrap (Table 2). Here, between two and ten species of GM, HexCer, CerP, PE-Cer, ST, as well as PI, PE, and PA species were identified (Figure 1C).

Human Aβ plaques are associated with alterations in sphingolipids

Previous studies using transgenic mouse models, have demonstrated Aβ plaque-specific enrichment and depletion of sphingolipid species including all identified GM, HexCer, CerP, PE-Cer and ST. To date, alterations of these species have not been demonstrated in human AD tissue at the level of a single Aβ plaque. Here, inspection of single ion images and bar plots of lipid signal distribution for individual plaques of verified lipid species revealed a general plaque-associated enrichment of GM, including GM1, GM2, and GM3 species with C18:0 (Figure 2A-C) and C20:0 (Supplemental Figure 2A-C) fatty acid (FA) moieties. Additionally, we also observed enrichment of a few neutral glycosphingolipids, including HexCer(30:1) and HexCer(32:1) (Supplemental Figure 2D, E). Lastly, CerP (d18:1/16:0), CerP (d18:1/18:0), and CerP (d18:1/20:0) (Figure 2D-F), as well as ceramide phospholipid conjugates, including PE-Cer(36:1), PE-Cer(38:1), and PE-Cer(40:1) (Figure 2G-I) were specifically enriched in the regions corresponding to the Aβ plaques. In accordance with previous reports from mice[6–8], the enrichment of these sphingolipids species was accompanied by a general depletion of signal corresponding to multiple sulfatides (ST, Figure 2J, K) and their hydroxylated isoforms (ST–OH) (Supplemental Figure 2F, G).

Human Aβ plaque are associated with alterations of phospholipids

We next set to investigate whether the phospholipid microenvironment changes suggested from transgenic mice studies were also reflected in the human subject Aβ plaques[6–8]. Indeed, inspection of loadings and corresponding single ion images and bar plots revealed that the observed PI, PE, and PA were present both as lysophospholipids (Lyso-), and polyunsaturated

fatty acids (PUFA), consistent with the animal studies. However, although the majority of the PUFA had AA or docosahexaenoic acid (DHA) residues, we observed clear differences in what specific lipid subspecies with AA/DHA localized to the Aβ plaque-pathology in the human subjects as compared to what has been reported for mice. In previous mouse studies we observed enrichment of Lyso-PIs, specifically LPI(16:0) and LPI(18:0) (Supplemental Figure 2A,B). However, these human samples instead show enrichment of LPI(20:4) (Supplemental Figure 2C). Further, just as for transgenic mice we also observed AA-containing PI(16:0/20:4) and PI(18:0/20:4), but in difference to mice, there was a lack of DHA-containing PI species (Figure 3A,B).

We next investigated the PE species present in the human tissue. Consistent with mice data we observed Lyso-PE species, specifically LPE(18:0) and LPE(22:6) (Supplemental Figure 2D, E). Among the PE species we observed plaque-specific enrichment of species previously reported in transgenic mice, including PE(18:1/18:0), and PE(18:1/20:0) (Supplemental Figure 2F,G), as well as the DHA-containing PE(18:0/22:6) (Figure 3C) and the plasmalogen PE(P-18:0/22:6) (Figure 3D). Additionally, we observed PE(16:0/22:6) (Supplemental Figure 2H). Consistent with the pattern of the PIs, we observed the AA-containing PE species not previously reported in mice. This included both PE(18:0/20:4) and PE(P-18:0/20:4) (Figure 3E, F).

Lastly, in context of human plaque pathology we observed cyclic phosphatidic acid (CPA), for the first time, specifically CPA(18:0) (Supplemental Figure 2I), and consistent with animal studies we observed PA(16:0/16:0) (Supplemental Figure 2J). However, in contrast to the animal studies we did not observe any AA-containing PA species, but instead found the DHA-containing PA(18:0/22:6) (Figure 3G).

Aβ plaque-associated sphingolipids and phospholipids correlate within class, but poorly between classes

Finally, chemical diversity within individual plaques has been reported, down to the level of individual lipid species[6,7]. Therefore, we endeavored to find any lipid species that co-localize more/less with one another. This would presumably indicate enrichment/depletion of specific metabolic pathways during distinct stages of the Aβ-plaque pathology progression. We performed SPSC within the areas corresponding to Aβ plaques for each of the PSEN patients. The correlation analysis revealed a general diversity of lipid colocalization patterns between patients (Figure 4A, B). Still, a broad pattern among the CerP and PE-Cer species could be observed in all of the patients. This colocalization pattern did to some extend correlate with HexCer, and to our surprise also GM1 species (Figure 4A-I, top red box). As suggested by the single ion images

and corresponding bar plots, there was a unique colocalization pattern present among the ST species (Figure 4A-II). The correlation of ST(d18:1/22:0) and its hydroxylated form was not as strong as among the other ST species. Lastly, there appeared to be a general co-localization of the phospholipid species, which appeared strongest for the AA and DHA residue containing PI, PE, and PA species (Figure 4A-III). Interestingly, PUFA moieties showed some colocalization with sphingolipid species, in particular CerP and PE-Cer (Figure 4A-III, bottom red box).

DISCUSSION

It has been previously shown that lipids play a central role in AD pathogenesis. AD-linked change in the levels of various lipid subclasses have been observed in cerebrospinal fluid, blood, and postmortem human brain tissue extracts [3,17,18]. Still, none of these studies provide a direct insight into possible local microenvironment changes that take place at the sites of Aβ plaque development. To overcome these limitations, chemical imaging approaches have been developed. The majority of these approached rely on MALDI-MSI that provides the molecular comprehensiveness and potential for specificity necessary to delineate the complexity of the lipid changes that take place in tissue. Still, these approaches have only been successfully applied in transgenic AD mouse models[7,8,16,19], and therefore do not negate the need for the analysis of postmortem human AD tissue.

In the current study, we performed pioneering analysis and verification of lipid microenvironment changes in postmortem human AD tissue from patients carrying *PSEN1* mutations. In detail, following comprehensive lipid analysis of postmortem brain tissue from five *PSEN1* mutation carrying AD patients, we verified the identity of these putatively assigned lipid species through complementary analysis using high mass resolution orbitrap instrumentation. In agreement with previous animal studies, we observed GM, HexCer, CerP, PE-Cer, and ST, as well as PI, PE, and PA species. The phospholipid species identified comprised both intact and lyso-forms [7,8,16,19].

Although we observed large differences in lipid signal enrichment within individual Aβ plaques between patients (bar plots for respective single ion images), when considering individual patients, the lipid signal was normally distributed and consistent within Aβ plaque ROIs. This is emphasized by both the bar plots and the SPSC for individual patients (Figure 4). The patterns could possibly be clearer if the postmortem tissues used in this study were from patients carrying the same *PSEN1* mutations, which was not the case (Table 1). Indeed, differences in the age-of-onset of clinical symptoms, Aβ plaque pathology distribution in the brain has been reported for various *PSEN1* mutations [20,21]. Therefore, despite the wide diversity in correlation strength between diverse lipid species, we observed general patterns that included a correlation of CerP,

PE-Cer, HexCer, and GM1 in every patient. Further, the phospholipid species displayed a general correlation that appeared strongest among the AA- and DHA-containing species. Together, these findings indicate that there might indeed be plaque-derived mechanistic patterns co-occurring with these lipid species.

Although the majority of the species present overlapped between previous animal studies and the human tissue analyzed here, we observed a clear difference in the increased number of AA- and DHA-containing species detected in human tissue. Additionally, the presence of these two residues depended on lipid subtype. Specifically, we observed almost exclusively AA-containing PIs, and AA-based lyso-PI. For PAs we observed mainly DHA-containing species. For PEs both AA and DHA species were observed.

Both AA and DHA are precursors of eicosanoids. Eicosanoids are essential for mediating inflammatory mechanisms of both astro- and microglia[22]. While AA is generally considered pro-inflammatory, DHA is believed to have the opposite effect. In the context of AD, the relevance of the increased presence of PIs and PAs ties back to involvement and sustained activity of triggering receptor expressed on myeloid cells 2 (TREM2) that has anionic lipid species, such as PI and PA, as its ligands[23]. On the other hand, changes in phospholipids have been linked to Aβ aggregation[3]. Although our study does not delineate the exact role the fatty acids residues and the lipid subtypes play in the molecular pathways of AD, it indicates that lipid subtype specific PUFAs are involved in the microenvironment occurrence and consequences of Aβ plaque pathology.

It is important to emphasize that this study is largely descriptive in nature, and hence no clear conclusion can be drawn, with respect to the limited number of cases used. Additionally, no elucidation of lipid isomers was performed. Still, the results obtained here will guide subsequent examinations and act as a demonstration of novel analytical approaches which are highly relevant for lipid studies of proteopathies.

CONCLUSIONS

In summary, this work is the first study of lipid microenvironment changes related to Aβ plaque pathology in postmortem human AD tissue. Here we provide spatially resolved single-ion patterns of multiple lipid classes (GM, CerP, PE-Cer, ST, PI, PE and PA) localizing to Aβ plaques. In addition to previous transgenic AD studies, this provides insight into potential phospholipid class-specific involvement in AD pathology progression. Overall, our work highlights the relevance and utility of multidimensional MSI as an aid in understanding molecular mechanisms of Alzheimer's disease.

Supporting Information

The Electronic Supporting Information including Table 1 and 2, as well as Supplemental Figures 1 and 2, are is available free of charge on the Journal's website.

AUTHOR INFORMATION

Author Contributions

WM and JH designed the study. WM, AB, SK performed experiments. WM and AB designed the analysis pipeline. WM, AB, KM analyzed the data. WM, AB, SK, KM, HZ, KB, TL, RH, and JH discussed the data. WM, AB and JH wrote the manuscript.

Funding Sources

WM is supported by an International Postdoc Grant of the Swedish Research Council VR (#2021-00478). JH is supported by the Swedish Research Council VR (#2018-02181 and #2019-02397), the Swedish Alzheimer Foundation (#AF-968238, #AF-939767, #AF- 980791) the National Institute of Health (NIH-NIA, R01AG078796, R21AG078538), Hjärnfonden (FO2022-0311), Magnus Bergvalls Stiftelse and Åhlén-Stiftelsen. (#213027). Stiftelsen Gamla Tjänarinnor (JH, HZ, KB), the Swedish Dementia Foundation (Demensfonden, JH, SK) and Gun och Bertil Stohnes Stiftelse (JH), are acknowledged for financial support.

HZ is a Wallenberg Scholar supported by grants from the Swedish Research Council (#2018-02532 and #2019-02397), the European Research Council (#681712 and #101053962), Swedish State Support for Clinical Research (#ALFGBG-71320), the Alzheimer Drug Discovery Foundation (ADDF), USA (#201809-2016862), the AD Strategic Fund and the Alzheimer's Association (#ADSF-21-831376-C, #ADSF-21-831381-C and #ADSF-21-831377-C), the Olav Thon Foundation, the Erling-Persson Family Foundation, Hjärnfonden, Sweden (#FO2019-0228), the European Union's Horizon 2020 research and innovation programme under the Marie Skłodowska-Curie grant agreement No 860197 (MIRIADE), the European Union Joint Programme – Neurodegenerative Disease Research (JPND2021-00694), and the UK Dementia Research Institute at UCL (UKDRI-1003). KB is supported by the Swedish Research Council (#2017-00915), the Alzheimer Drug Discovery Foundation (ADDF), USA (#RDAPB-201809-2016615), the Swedish Alzheimer Foundation (#AF-930351, #AF-939721 and #AF-968270), Hjärnfonden, Sweden (#FO2017-0243 and #ALZ2022-0006), the Swedish state under the agreement between the Swedish government and the County Councils, the ALF-agreement (#ALFGBG-715986 and #ALFGBG-965240), the European Union Joint Program for

Neurodegenerative Disorders (JPND2019-466-236), the National Institute of Health (NIH), USA, (grant #1R01AG068398-01), and the Alzheimer's Association 2021 Zenith Award (ZEN-21-848495).

Notes

The authors declare no competing interests.

ACKNOWLEDGMENT

We thank the staff at Centre for Cellular Imaging (CCI), Core Facilities, The Sahlgrenska Academy, University of Gothenburg, and the National Microscopy Infrastructure, NMI (VR-RFI 2019-00022), for help with development of imaging paradigm and microscopy expertise.

ABBREVIATIONS

Arachidonic acid (AA), Alzheimer's disease (AD), amyloid-β (Aβ), ceramide-1-phosphate (CerP), docosahexaenoic acid (DHA), famillial Alzheimer's disease (fAD), monosialo-ganglioside (GM), ceramide monohexoside (HexCer), matrix assisted laser desorption/ionization (MALDI), mass spectrometry imaging (MSI), phosphatidylethanolamine (PE), ceramide phosphoethanolamine conjugate (PE-Cer), phosphoinositol (PI), presenilin (PSEN), polyunsaturated fatty acid (PUFA), sulfatide (ST).

FIGURES AND TABLES

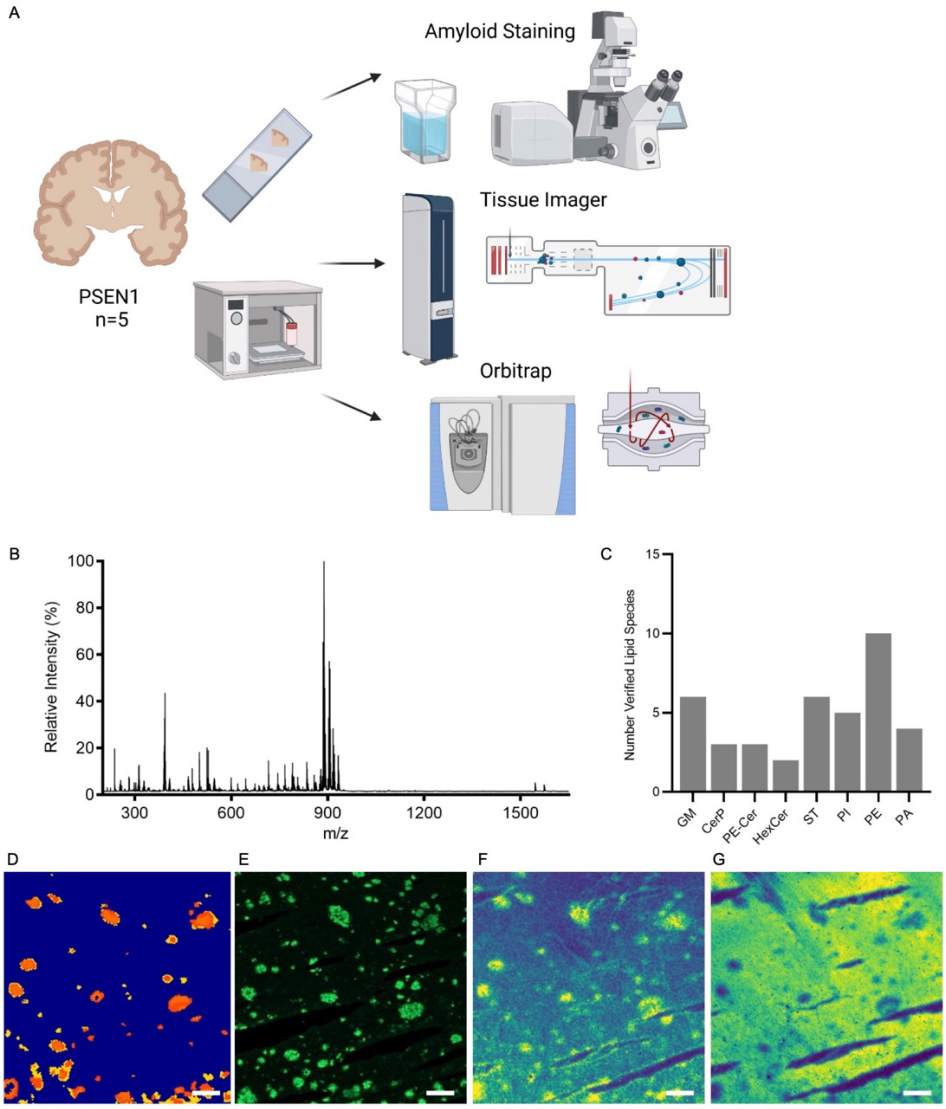

Figure 1. Setup for chemical analysis of sphingolipids and phospholipids in postmortem human AD tissue of patients with *PSEN 1* mutations. (A) Schematic of setup of this study where frozen postmortem tissue from five *PSEN1* mutation carrying patients (labeled PSEN1-5) was consecutively cryo-sectioned on conductive ITO glasses and used for either amyloid staining to identify Aβ plaque pathology (top) or sprayed with a chemical matrix for lipid analysis using tissue-imager RapiFlex (middle) or high-mass resolution orbitrap (bottom) (Created with BioRender.com) (B) Average mass spectra of Aβ plaques from one of the *PSEN1* patients. (C) Bar plot representing the numbers of verified lipid species grouped by subtype. (D) Spatial segmentation by k-means clustering allowed for identification of Aβ plaque like regions of interests (ROIs). The identity of these ROIs as Aβ plaques was confirmed through (E) amyloid staining. This staining (E) overlapped well both with the clustering (D), but even better single ion images of enriched species such as (F) monosialo-ganglioside GM1(d18:1/20:0), and depleted species such as (G) sulfatide ST(d18:1/24:0). Scalebar: 150 µm.

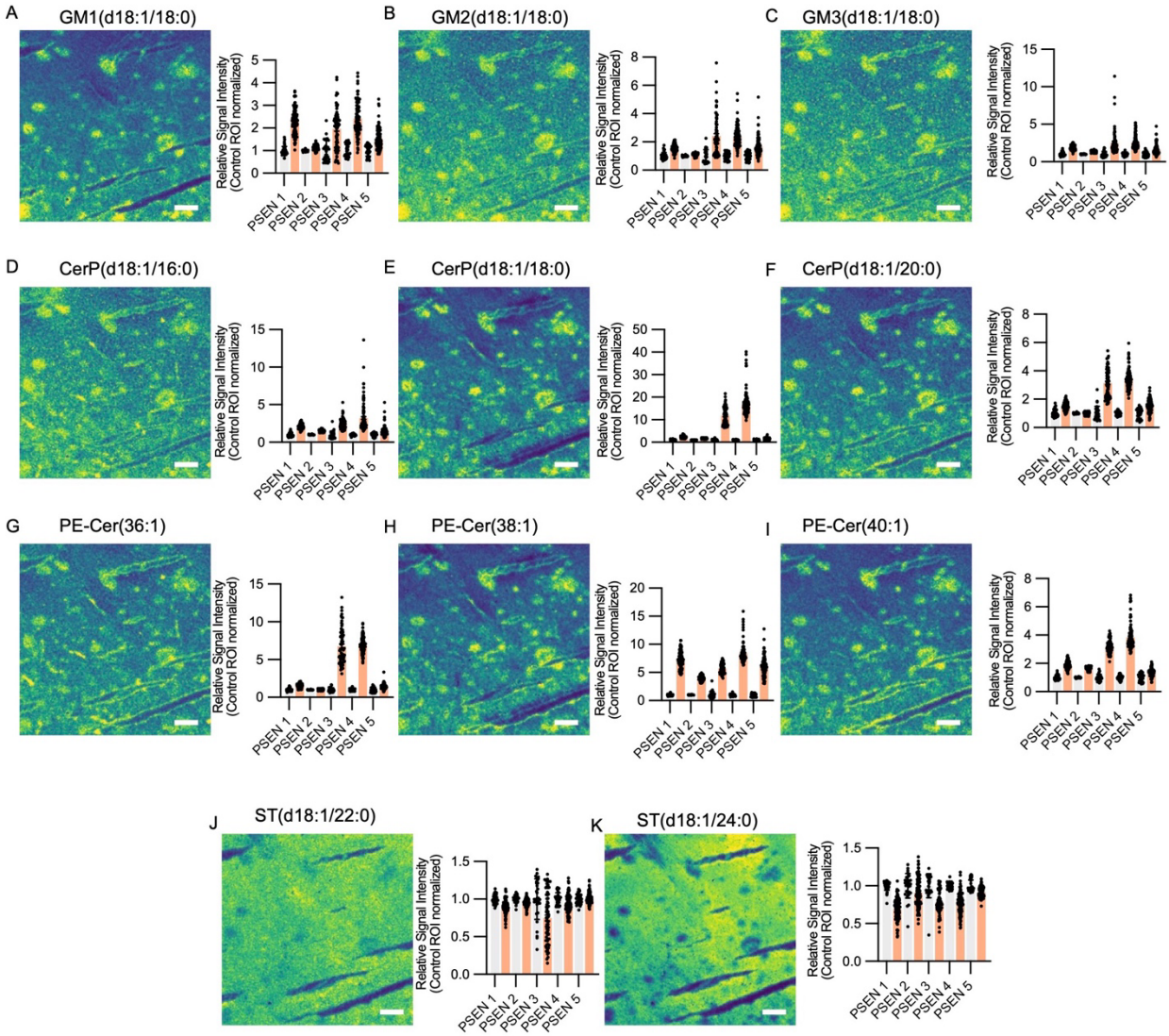

Figure 2. MALDI MSI of sphingolipids in postmortem human AD tissue of patients with *PSEN1* mutations. The Aβ plaque pathology is associated with local enrichment and depletion of several sphingolipids as apparent by the single ion images (left) and corresponding single Aβ plaque relative signal enrichment (right) of monosialo-gangliosides (GM), including (A) GM1(d18:1/18:0), (B) GM2(d18:1/18:0), and (C) GM3(d18:1/18:0). Similar Aβ plaque pathology specific enrichment is also present for ceramide-1-phosphates (CerP) and ceramide phosphoethanolamine conjugates (PE-Cer), including (D) CerP (d18:1/16:0), (E) CerP (d18:1/18:0), (F) CerP (d18:1/20:0), respective (G) PE-Cer(36:1), (H) PE-Cer(38:1), (I) PE-Cer(40:1). On the other side there appears to be a Aβ plaque depletion of sulfatides including (J) ST(d18:1/22:0) and (K) ST(d18:1/24:0). Signal intensities from ca 100 Aβ plaques/patient was extracted for the barplots. Scalebar: 150 µm.

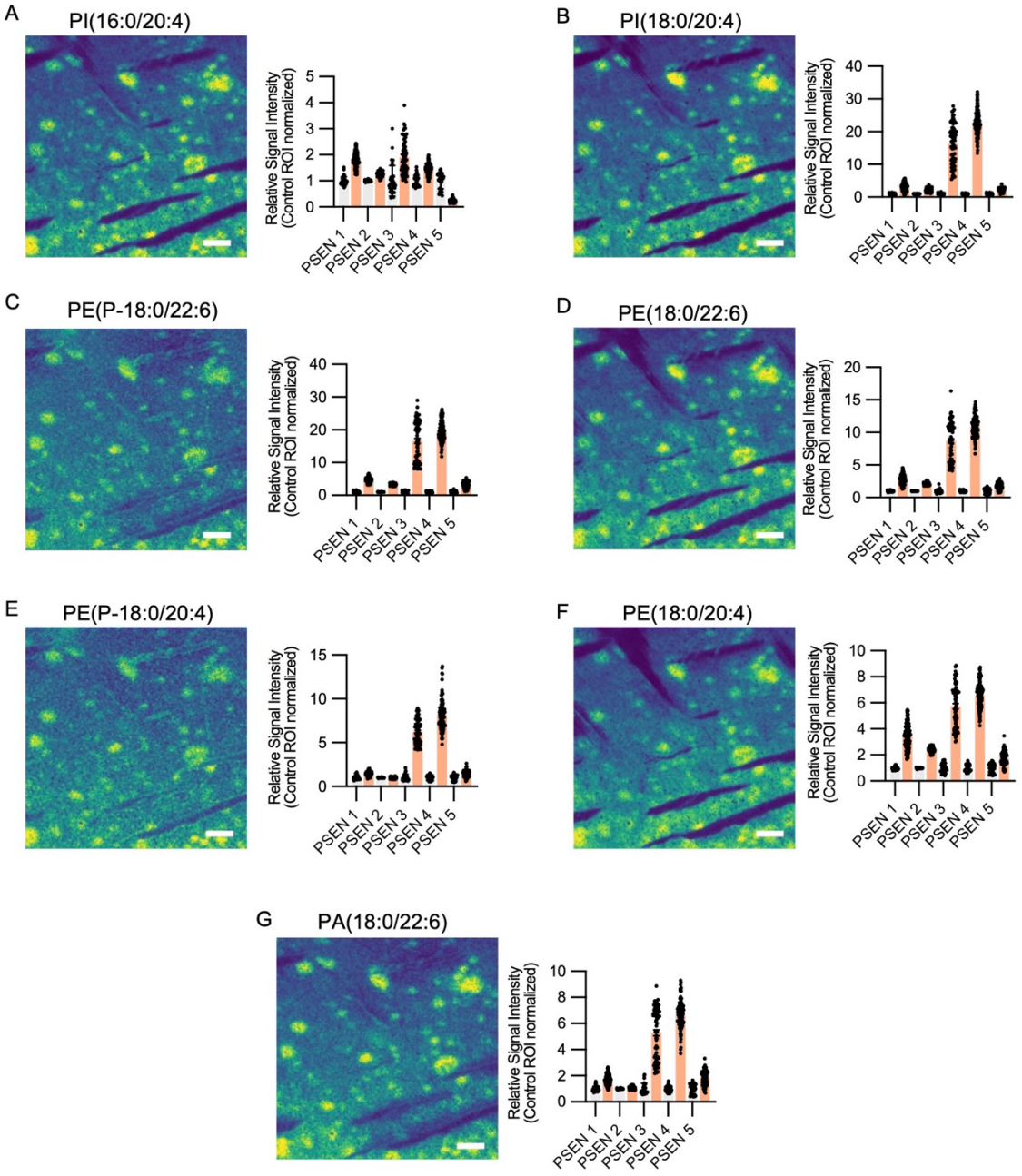

Figure 3. MALDI MSI of phospholipids in postmortem human AD tissue of patients with *PSEN1* mutations. The Aβ plaque pathology is associated with alterations of arachidonic acid (AA) or docosahexaenoic acid (DHA) containing phospholipids as apparent by the single ion images (left) and corresponding single Aβ plaque relative signal enrichment (right). This includes arachidonic acid (AA) residue containing phosphatidylinositoles, such as (A) PI(16:0/20:4) and (B) PI(18:0/20:4). Similar Aβ plaque pathology specific enrichment is also present for DHA containing phosphatidylethanolamine (C) PE(18:0/22:6) and plasmogen (D) PE(P-18:0/22:6), as well as the AA containing (E) PE(18:0/20:4) and (F) PE(P-18:0/20:4).We also observed enrichment of DHA containing phosphatidic acid, PA(18:0/22:6). Signal intensities from ca 100 Aβ plaques/patient was extracted for the barplots. Scalebar: 150 µm.

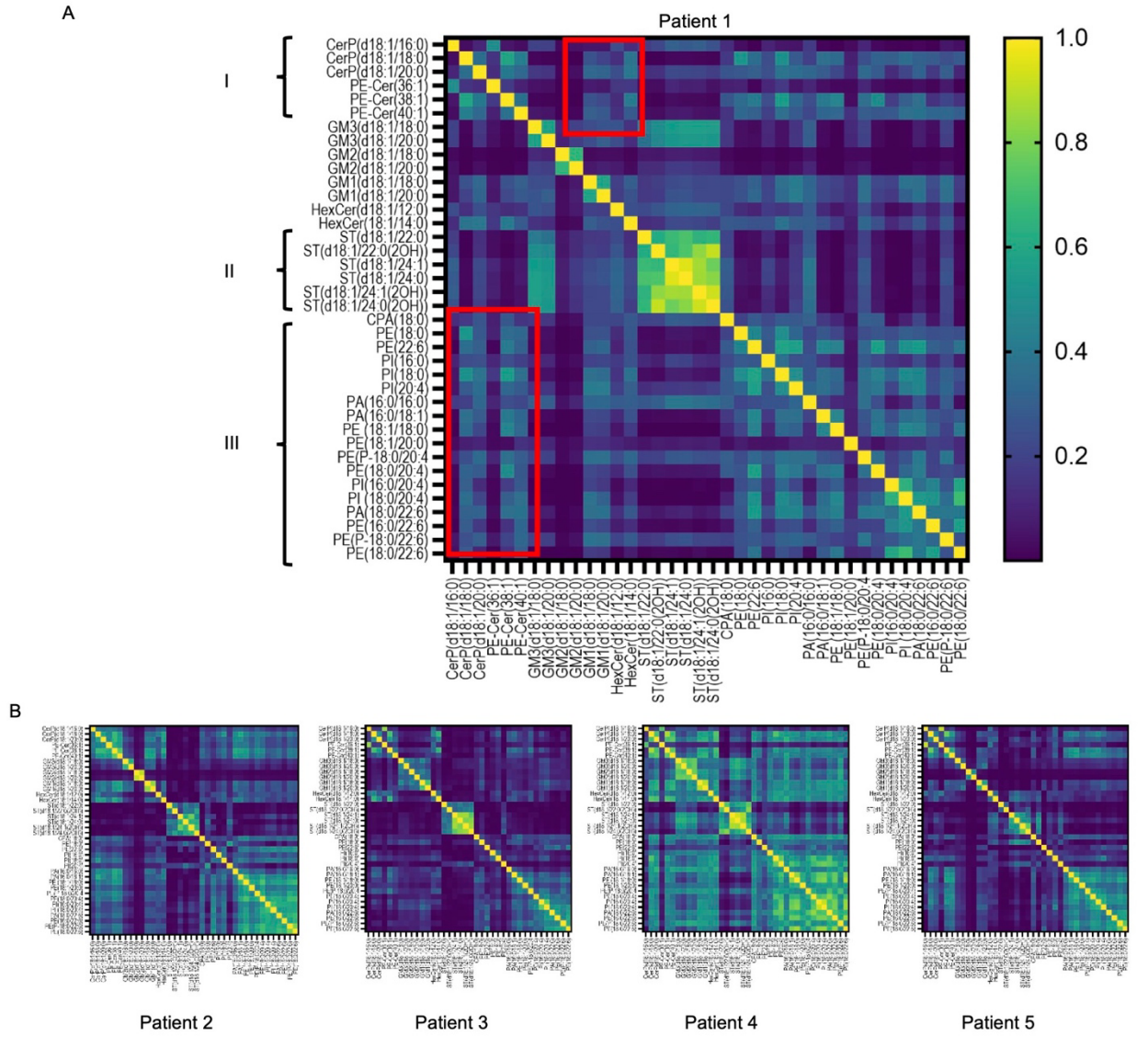

Figure 4. Heatmap representing single pixel signal correlation (SPSC) between individual sphingolipid and phospholipid for all of the *PSEN1* mutation carriers. (A, B) similar correlation patterns were present among the patiens, but with varying degree of correlation strength. (A-I) We observed an interesting correlation pattern of ceramide-1-phosphates (CerP) and ceramide phosphoethanolamine conjugates (PE-Cer) with (A-I, top red box) not only ceramide monohexosides (HexCer), but also the longest monosialo-gangliosides (GM), the GM1 species. (A-II) There was a colocalization pattern between sulfatides (ST), both in the hydroxylated and non-hydroxylated form. (A-III) Lastly, in addition to the general correlation among phospholipid species, that was strongest for those species that contain the arachidonic acid (AA) or docosahexaenoic acid (DHA) residues, (A-III, bottom red box) there was some colocalization of the phospholipid species with sphingolipid species, in particular CerP and PE-Cer.

Table 1. Patient chart summarizing the demographics and diagnostic scores of PSEN1 familial AD cased used in the study

Patient	Mutation	Gender	Age at onset	Age at Death	Duration	Clinical diagnosis	Pathological diagnosis	Braak tau	Thal phase	CERAD	ABC
1	PS1 A434T & T291A	M	42	47	5	FAD	FAD	5	5	3	A3B3C3
2	PS1 R278I	F	46	65	19	FAD	FAD	6	5	3	A3B3C3
3	PS1 L250S	M	47	58	11	FAD	FAD	6	5	3	A3B3C3
4	PS1 E120K exon 5	F	31	37	6	FAD	FAD	6	5	3	A3B3C3
5	PS1 E184D	F	45	58	13	FAD	FAD	6	5	3	A3B3C3

Table 2.

Lipid Class	Common Lipid Name	Theor. Mass	Observed Mass $[M-H]^-$ (MALDI TOF)	Observed Mass $[M-H]^-$ (Orbitrap)
CerP	CerP(d18:1/16:0)	617,4784	616,453	616,4712
CerP	CerP(d18:1/18:0)	645,5097	644,421	644,5025
CerP	CerP(d18:1/20:0)	673,5410	672,483	672,5339
Cer-PE	PE-Cer(36:1)	688,5519	687,496	687,5443
Cer-PE	PE-Cer(38:1)	716,5832	715,565	715,5757
Cer-PE	PE-Cer(40:1)	744,6145	743,509	743,6070
GM	GM3(d18:1/18:0)	1180,7445	1179,599	1179,7366
GM	GM3(d18:1/20:0)	1208,7758	1207,63	1207,7683
GM	GM2(d18:1/18:0)	1383,8238	1382,717	1382,8153
GM	GM2(d18:1/20:0)	1411,8551	1410,756	1410,8457
GM	GM1(d18:1/18:0)	1545,8767	1544,733	1544,8679
GM	GM1(d18:1/20:0)	1573,9080	1572,818	1572,8992
HexCer	HexCer(d18:1/12:0)	643,5023	642,394	-
HexCer	HexCer(18:1/14:0)	671,5336	670,464	-
PA	CPA(18:0)	420,2641	419,251	419,2569
PA	PA(16:0/16:0)	648,4730	647,445	-

PA	PA(16:0/18:1)	672,4730	673,441	673,4813
PA	PA(18:0/22:6)	748,5043	747,469	747,4970
PE	PE(18:0)	481,3168	480,245	480,3096
PE	PE(22:6)	525,2855	524,247	524,2785
PE	PE (18:1/18:0)	745,5622	744,523	744,5548
PE	PE(18:1/20:0)	773,5935	772,467	-
PE	PE(P-18:0/20:4)	751,5516	750,525	750,5444
PE	PE(18:0/20:4)	767,5465	766,559	766,5395
PE	PE(16:0/22:6)	763,5152	762,403	762,5078
PE	PE(P-18:0/22:6)	775,5516	774,47	774,5444
PE	PE(18:0/22:6)	791,5465	790,449	790,5392
PI	PI(16:0)	572,2962	571,242	-
PI	PI(18:0)	600,3275	599,274	599,3203
PI	PI(20:4)	620,1377	619,258	619,2890
PI	PI(16:0/20:4)	858,5258	857,414	857,5185
PI	PI (18:0/20:4)	886,5571	885,468	-
ST	ST(d18:1/22:0)	863,6156	862,513	862,6080
ST	ST(d18:1/22:0(2OH))	879,6106	878,539	878,6033
ST	ST(d18:1/24:1)	889,6313	888,54	888,6238
ST	ST(d18:1/24:0)	891,6469	890,559	890,6398
ST	ST(d18:1/24:1(2OH))	905,6262	904,543	904,6187
ST	ST(d18:1/24:0(2OH))	907,6419	906,57	906,6346

REFERENCES

1. Knopman, D. S. *et al.* Alzheimer disease. *Nat. Rev. Dis. Prim.* **7**, 33 (2021).
2. Aisen, P. S., Jimenez-Maggiora, G. A., Rafii, M. S., Walter, S. & Raman, R. Early-stage Alzheimer disease: getting trial-ready. *Nat. Rev. Neurol.* (2022) doi:10.1038/s41582-022-00645-6.
3. Di Paolo, G. & Kim, T.-W. Linking Lipids to Alzheimer's Disease: Cholesterol and Beyond. *Nat. Rev. Neurosci.* **12**, 284–296 (2011).
4. Liu, C.-C., Kanekiyo, T., Xu, H. & Bu, G. Apolipoprotein E and Alzheimer disease: risk, mechanisms and therapy. *Nat Rev Neurol* **9**, 106–118 (2013).
5. Bellenguez, C. *et al.* New insights into the genetic etiology of Alzheimer's disease and related dementias. *Nat. Genet.* **54**, 412–436 (2022).
6. Michno, W., Wehrli, P. M., Zetterberg, H., Blennow, K. & Hanrieder, J. GM1 locates to mature amyloid structures implicating a prominent role for glycolipid-protein interactions in Alzheimer pathology. *BBA Proteins Proteom* **1867**, 458–467 (2019).
7. Michno, W. *et al.* Multimodal Chemical Imaging of Amyloid Plaque Polymorphism Reveals Abeta Aggregation Dependent Anionic Lipid Accumulations and Metabolism. *Anal Chem* **90**, 8130–8138 (2018).
8. Kaya, I. *et al.* Delineating Amyloid Plaque Associated Neuronal Sphingolipids in Transgenic Alzheimer's Disease Mice (tgArcSwe) Using MALDI Imaging Mass Spectrometry. *ACS Chem Neurosci* (2017) doi:10.1021/acschemneuro.6b00391.
9. Montine, T. J. *et al.* National Institute on Aging–Alzheimer's Association guidelines for the neuropathologic assessment of Alzheimer's disease: a practical approach. *Acta Neuropathol.* **123**, 1–11 (2012).
10. Klingstedt, T. *et al.* Synthesis of a library of oligothiophenes and their utilization as fluorescent ligands for spectral assignment of protein aggregates. *Org Biomol Chem* **9**, 8356–8370 (2011).
11. Nyström, S. *et al.* Evidence for age-dependent in vivo conformational rearrangement within Abeta amyloid deposits. *ACS Chem Biol* **8**, 1128–1133 (2013).
12. Belov, M. E. *et al.* Design and Performance of a Novel Interface for Combined Matrix-Assisted Laser Desorption Ionization at Elevated Pressure and Electrospray Ionization with Orbitrap Mass Spectrometry. *Anal. Chem.* **89**, 7493–7501 (2017).
13. Schramm, T. *et al.* imzML — A common data format for the flexible exchange and processing of mass spectrometry imaging data. *J. Proteomics* **75**, 5106–5110 (2012).
14. Chambers, M. C. *et al.* A cross-platform toolkit for mass spectrometry and proteomics. *Nat.*

Biotechnol. **30**, 918–920 (2012).

15. Fahy, E., Sud, M., Cotter, D. & Subramaniam, S. LIPID MAPS online tools for lipid research. *Nucleic Acids Res.* **35**, W606–W612 (2007).
16. Michno, W. *et al.* Structural amyloid plaque polymorphism is associated with distinct lipid accumulations revealed by trapped ion mobility mass spectrometry imaging. *J. Neurochem.* **160**, 482–498 (2022).
17. Chan, R. B. *et al.* Comparative Lipidomic Analysis of Mouse and Human Brain with Alzheimer Disease. *J. Biol. Chem.* **287**, 2678–2688 (2012).
18. van der Velpen, V. *et al.* Systemic and central nervous system metabolic alterations in Alzheimer's disease. *Alzheimers. Res. Ther.* **11**, 93 (2019).
19. Kaya, I. *et al.* Novel Trimodal MALDI Imaging Mass Spectrometry (IMS3) at 10 mum Reveals Spatial Lipid and Peptide Correlates Implicated in Abeta Plaque Pathology in Alzheimer's Disease. *ACS Chem Neurosci* **8**, 2778–2790 (2017).
20. Petit, D. *et al.* Aβ profiles generated by Alzheimer's disease causing PSEN1 variants determine the pathogenicity of the mutation and predict age at disease onset. *Mol. Psychiatry* **27**, 2821–2832 (2022).
21. Willumsen, N. *et al.* Variability in the type and layer distribution of cortical Aβ pathology in familial Alzheimer's disease. *Brain Pathol.* **32**, e13009 (2022).
22. Xu, D. *et al.* Increased arachidonic acid-containing phosphatidylcholine is associated with reactive microglia and astrocytes in the spinal cord after peripheral nerve injury. *Sci Rep* **6**, 26427 (2016).
23. Wang, Y. *et al.* TREM2 lipid sensing sustains the microglial response in an Alzheimer's disease model. *Cell* **160**, 1061–1071 (2015).